LARGE EDDY SIMULATIONS OF MIXING IN THE WALL REGION OF AN IMPINGING JET

J. Revstedt
Division of Fluid Mechanics, Lund Institute of Technology
P.O. Box 118, S-221 00 Lund, Sweden

F. Guillard
Division of Food Engineering, Lund Institute of Technology
P.O. Box 118, S-221 00 Lund, Sweden

L. Fuchs
Division of Fluid Mechanics, Lund Institute of Technology
P.O. Box 118, S-221 00 Lund, Sweden

C. Trägårdh
Division of Food Engineering, Lund Institute of Technology
P.O. Box 118, S-221 00 Lund, Sweden

ABSTRACT

Large eddy simulations of a circular jet impinging on a flat plate have been carried out. The distance between the jet nozzle and the plate was varied between 2 and 6 nozzle diameters and the Reynolds number was 10000. The aim of the work is by using large eddy simulations study the mixing properties and how they are influenced by the nozzle to wall distance in the region close to the impingment wall.
The computational code is a multi-grid finite difference code using a staggered grid. The results show that turbulence level close to the stagnation point is substantially increased when the impingement distance exceeds 4.0 nozzle diameters. However, this seem to have little effect on the maximum level of concentration fluctuations in the developing wall jet.

INTRODUCTION

The impinging jet is used in many industrial applications where mixing is of importance such as enhancing the cooling and heating of surfaces, combustion and mixing processes in chemical and biochemical industry. It is also suitable as a test case for turbulence models since the impinging jet invokes several fluid dynamical phenomena which a k-ε turbulence model cannot handle, e.g. stagnation point and strong stream line curvature. Such studies have been performed by Craft *et al.* (1993) using the measurement data of Cooper *et al.* (1993). The found an over all poor performance of the standard k-ε model and the standard Reynolds stress models. This was also noted by Behnia *et al.* (1996). They found that the k-ε model and the standard Reynolds stress models gave poor agreement with measurements.
Recently, LES of a circular impinging jet were made by Olsson and Fuchs (1998) who studied the effects of different sub grid scale (SGS) models. The effects of SGS models on the mixing were studied by Revstedt *et al.* (1998)
In this work the main focus has been on using LES to investigate the mixing process in the impingement region, i.e. close to the stagnation point and in the beginning of the wall jet, and its dependence on the nozzle to wall distance. In the ealier studies by Revstedt and Fuchs (1997) and Revstedt *et al.* (1998) an isotropic Cartesian grid was used. Consequently the near wall flow could not be predicted with any accuracy due to low resolution. By using a stretched grid we are now able to study also the development of the wall jet. The results are also compared to Planar Laser Induced Fluorescence (PLIF) measurements of the concentration levels.

GOVERNING EQUATIONS

LES is based on spatial filtering of the equations of motion rather than time averaging used in traditional turbulence modelling. The space filtering of a function $f(x_i,t)$ is defined as

$$\overline{f(x_i,t)} = \int_{-\infty}^{\infty} G(x_i - x_i')f(x_i',t)dx_i' \quad (1)$$

where G is a filter function.
The space filtered non-dimensionalized equations for the conservation of mass and momentum for an incompressible Newtonian fluid can be written, using summation convention, as

$$\frac{\partial \overline{u_i}}{\partial x_i} = 0 \quad (2)$$

$$\frac{\partial \overline{u_i}}{\partial t} + \overline{u_j}\frac{\partial \overline{u_i}}{\partial x_j} = -\frac{\partial \overline{p}}{\partial x_i} + \frac{1}{\mathrm{Re}}\frac{\partial}{\partial x_j}\frac{\partial \overline{u_i}}{\partial x_j} - \frac{\partial \tau_{ij}}{\partial x_j} \quad (3)$$

$$\tau_{ij} = \overline{u_i u_j} - \overline{u_i}\,\overline{u_j} \quad (4)$$

where τ_{ij} is the Sub Grid Scale (SGS) stress tensor, which reflects the effect of the
unresolved scales on the resolved scales. Since this tensor contains correlations of unfiltered velocities which are not explicitly known it has to be modelled. Usually the unresolved scales are modeled using the resolved quantities. However, as a first approximation one may take advantage of the properties of the numerical schemes. In the computational code used the convective terms are approximated by third order upwind finite differences. The truncation error from this approximation acts dissipatively, at least in an averaged sense, draining energy from the resolved scales. It has been reported by Gullbrand *et al.* (1998) that the energy flux caused by artificial (numerical) dissipation also can allow for some back scatter. Also, it has been shown by Olsson and Fuchs (1994) for a free jet that this term is of the same order and located in the same area as the SGS-term in a Smagorinsky model. Good results using implicit modelling of the flow around a cylinder at high Reynolds numbers were obtained by Kawamura and Kuwahara (1984). However, it should be noted that for a given grid resolution the turbulent properties are improved by using explicit SGS models, e.g. Revstedt *et al.* (1998).

PASSIVE SCALAR TRANSPORT

For the concentration of an inert additive, c, the filtered transport equation can be written as

$$\frac{\partial \overline{c}}{\partial t} + \overline{u_j}\frac{\partial \overline{c}}{\partial x_j} = \frac{1}{\mathrm{Re}\,Sc}\frac{\partial}{\partial x_j}\frac{\partial \overline{c}}{\partial x_j} - \frac{\partial \psi_j}{\partial x_j} \quad (5)$$

where Sc = ν/D is the Schmidt number. In this work the molecular diffusion is assumed to be much
smaller than the convective and turbulent transport and therefore neglected.
For liquid-liquid mixing usually Sc ≈1000.
The factor ψ_j in equation (6) is SGS mixing defined as:

$$\psi_j = \overline{u_j c} - \overline{u_j}\,\overline{c} \quad (6)$$

The factor ψ_j has to be modelled since it too contains correlations between non-filtered variables. The same approach as for the SGS stress tensor has been applied, i.e. we use the discretization truncation errors (numerical diffusion) to account for the SGS mixing.

NUMERICAL METHOD

The spatial discretisation of the governing equations is performed on a Cartesian staggered grid. The convective terms are discretised using the third order upwind scheme by Rai and Moin (1991). A fourth order central difference scheme was used for all other term (Olsson and Fuchs, 1998). Time intgration is done by a four step explicit Runge-Kutta type scheme. A Poisson equation is solved for the pressure correction. To accleterate the solution of this equation a multi grid method is used.
The transport equation for concentration is solved only on the finest multi-grid level by using a coverged velocity field. However, in order to avoid unphysical oscillations in the solution the spatial discretization is done by a hybrid scheme giving first or second order accuracy depending on the cell Reynolds number.
To achieve higher grid resolution near the impingment wall we use the analytical grid stretching function by Olsson and Fuchs (1998). The advantage of using an analytical function is that exact expressions for the derivatives used in the coordinate transformations can be calculated.

BOUNDARY CONDITIONS

No-slip conditions are set on all walls. At the jet nozzle both the velocity and the
concentration was set to a "top-hat" profile. A random perturbation of 5 % of the average inlet velocity was superimposed on the nozzle velocity in all directions. At the outlet a Neumann condition corrected to ensure global mass conservation was applied.
The concentration of the inert additive was set to unity at the nozzle and to zero on the wall, on the outlet boundaries a Neumann condition was used.

GEOMETRICAL SET-UP

The simulation were made on a semi confined impinging jet as shown in Figure 1. The impingment distance D_{pw} was varied between 2 and 6 nozzle diameters (D_0). The grid

sizes and resolution are given in Table 1. The temporal resolution is specified in terms of CFL number to 0.8.

Table 1. Geometry size and grid resolution

D_{pw}/D_0	Grid size	h_x, h_z	h_y
2.0	96×48×96	0.0833	0.17-0.005
4.0	96×96×96	0.0833	0.17-0.005
4.8	96×120×96	0.0833	0.17-0.005
6.0	96×148×96	0.0833	0.17-0.005

RESULTS

The circular impinging jet consists mainly of three parts: The developing jet, the impingement region and the radial wall jet. The developing jet exhibits both axis-symmetry and spiral instabilities. These instabilities generate large coherent structures which are convected down stream causing unsteady separation in the wall jet region (Didden and Ho, 1985). Didden and Ho (1985) used a forcing of the jet causing certain frequencies of the instabilities to be amplified. It was shown by Olsson and Fuchs (1997) that even in the unforced case, which is the one presented in this paper, a frequency around Strouhal number of 0.3 and its harmonics are the first to grow in the shear layer. One could therefore expect to see the unsteady separation also in the unforced case at least at small D_{pw}.

In the developing jet part, at short distances (up to about 4 D_0), turbulence cannot fully develop (unless it is already developed within the nozzle) before the wall affects the jet. This effect is illustrated in Figure 2 showing the turbulent kinetic energy along the jet centreline for the nozzle to wall distances considered. A dramatic increase in turbulence level is seen when D_{pw} is increased from 4 to 4.8 which, as will be shown below, has only a limited influence on the mixing behaviour in the near wall part of the impingement region.

The influence of this on the mixing can be seen from Figure 3. This figure shows the average concentration and the concentration fluctuations as a function of radius at 1.0 D_{pw} from the wall, i.e. just after the jet enters the impingment zone. As would be expected the mean profile of concentration becomes wider as D_{pw} is increased. Also, a substantial increase in fluctuation level is observed up to $D_{pw} = 4.8$.

Studying the rms of concentrations at several positions one can see that close to the jet center line ($r / D_0 = 1.0$) there is a region of high values of c_{rms} ranging between $x/D_0 = 0.1$ and $x/D_0 = 0.3$ (Figures 4 and 5). The magnitude of the concentration fluctuations seems to decrease somewhat with increasing D_{pw}. The major difference is when D_{pw} is increased from 4.0 to 4.8 the region of high fluctuation grows substantially. As a comparison we have added results obtained by Planar Laser Induced Fluorecesce (PLIF) using the methodology described by Guillard *et al.* (1998) and also LES results using a dynamic SGS model (Revstedt *et al.*, 1998), both for $D_{pw} = 4.8$.

This also affects the mean concentration giving wider profiles with lower maximum value for $D_{pw} = 4.8$ (Figures 6 and 7). Studying the maximum value of concentration fluctuations along the radial direction, depicted in Figure 8, one can see that beyond $r/D_0 = 1.0$ the levels are not very different when changing D_{pw} but a slight decrease in $c_{rms,max}$ with increasing D_{pw} can be detected. Also at $r/D_0 = 3.0$ there seems to be at decrease in $c_{rms,max}$ regardless of the impingement distance.

The influence of the coherent structures on the mixing process near the wall is evident from Figures 9 and 10, which show the instantaneous velocity and concentration fields in an area $r/D_0 = 2.0$ to 3.0 and \$ $x/D_0 = 0.0$ to 1.0 for $D_{pw} = 4.0$. The primary vortex lifts the boundary layer generating a seperation and a secondary vortex, as reported by Olsson and Fuchs (1998). These vortices contribute to the mixing by lifting areas of high concentration from the wall. However, the concentration levels closest to the wall seem to be only slightly affected by the separation.

Figures 11 and 12 depicts the Fourier transform of the concentration fluctuations for $D_{pw} = 2.0$ and $D_{pw} = 4.0$ respectively. For the shorter impingement distance one observes a distinct peaks at St ≈0.28 and St ≈ 0.52 at the point closest to the jet center line. A leats the first one of these most probably originates from the shear layer inastability in the developing jet. Further down stream ($r/D_0 = 3.0$) the fluctuations are shifted towards lower frequencies and no distinct peaks can be observed. Increasing the impingement distance to 4.0 D_0 the same trend is observed however only one distinct peak (St ≈0.37) is detected.

CONCLUSIONS

Large eddy simulations of a jet impinging on a flat plate were performed. The simulation results agree well with experimental data. The average concentration profiles in the early part of the radial wall jet are to a large extent influenced by the nozzle to wall distance, i.e. increased distance gives a wider profile with lower maximum value. The concentration fluctuations does not seem to be affected to the same extent, however a marginal decrease is observed with increasing impingement distance. At shorter distances the scalar transport is to a large extent governed by low frequency vortex structures, at least close to the stagnation point. As the distance is increased the developing turbulence plays a increasingly important role in the mixing.

ACKNOWLEDGMENTS

The authors gratefully acknowledge the financial support for this work by the EU through the Biotechnology Programme of Framework IV. This work is a part of the project 'Bioprocess Scale-up Strategy', project no. BIO-CT95-0028.

REFERENCES

Behnia, M., Parneix, S. and Durbin, P., 1996, "Simulation of jet impingment heat transfer with the k - ε - v^2 model", In Annual Research Briefs, pp. 3-16., Center For Turbulence Research, Stanford University.

Cooper, D., Jackson, D.C., Launder, B.E. and Liao, G.X., 1993, "Impinging jet studies for turbulence model assessment-I. Flow-field experiments", *int. J. Heat Mass Transfer*, vol. 10, pp. 2675—2684.

Craft, T.J., Graham, L.J.W., and Launder, B.E.. 1993, "Impinging jet studies for turbulence model assessment-II. An examination of the performance of four turbulence models", *int. J. Heat Mass Transfer*, vol. 10, pp.2685--2697.

Didden, N. and Ho, C.-M., 1985, "Unsteady separation in a boundary layer produced by an impinging jet" *J. Fluid Mech.*, vol. 160, pp.235--256.

Guillard, F., Fritzon, R., Revstedt, J., Trägårdh, C.,Aldén, M. and Fuchs, L., 1998, "Mixing in a confined turbulent impinging jet using Planar Laser-Induced Fluorescence", *Experiments in Fluids*, vol. 25, pp.143--150.

Gullbrand, J. Bai, X.-S. and Fuchs, L., 1998, "Large eddy simulation of turbulent reacting flows using Cartesian grid and boundary corrections", *AIAA paper*, no. 98-3317.

Kawamura, T. and Kuwahara, K., 1984, "Computation of high Reynolds number flow around a circular cylinder with surface roughness", *AIAA paper*, no. 84-0340.

Olsson, M. and Fuchs, L., 1994, "Significant terms in dynamic SGS-modeling", *Direct and Large Eddy Simulations I.* P.R. Voke et al., ed., Kluwer Academic Publishers.

Olsson, M. and Fuchs, L., 1997, "Amplified frequencies and SGS-models effects in the proximal region a circular jet", *Direct and Large Eddy Simulations II*, P.R. Voke et al., ed., Kluwer Academic Publishers.

Olsson, M. and Fuchs, L., 1998, "Large eddy simulations of a forced semiconfined circular impinging jet", *Phys. Fluids*, vol. 10, no. 2, pp. 476--486.

Rai, M.M. and Moin, P., 1991, "Direct simulations of turbulent flow using finite-difference schemes", *J. Comput. Phys.*, vol. 96, no. 15.

Revstedt, J. and Fuchs, L., 1997, "Large eddy simulations of turbulent flow and mixing in an impinging jet" ,*Numerical Methods in laminar and turbulent flow*, vol. X, pp. 673-682, C. Taylor and J. Cross, ed., Pineridge Press Swansea, UK.

Revstedt,, J., Gullbrand, J., Guillard, F., Fuchs, L. and Trägårdh, C., 1998, "Large eddy simulations of mixing in an impinging jet", *Proceedings of the 4th ECCOMAS Computational Fluid Dynamics Conference*}}, K.D. Papailiou et al., ed., pp. 1169-1174. John Wiley & Sons.

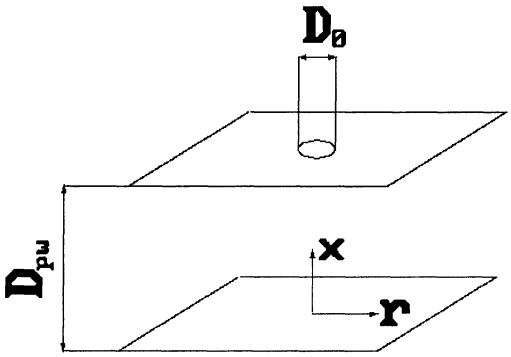

Figure 1. Simulation geometry and coordinate system

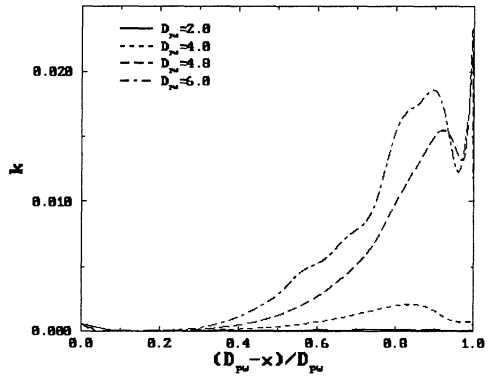

Figure 2. Turbulent kinetic energy at the jet centreline

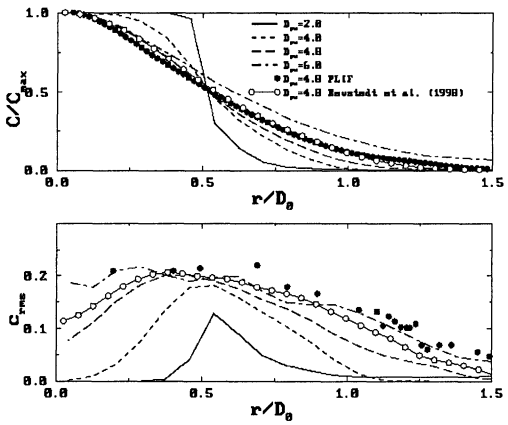

Figure 3.Average concentration and rms. of concentration fluctuations at 1.0 D_0 from the wall

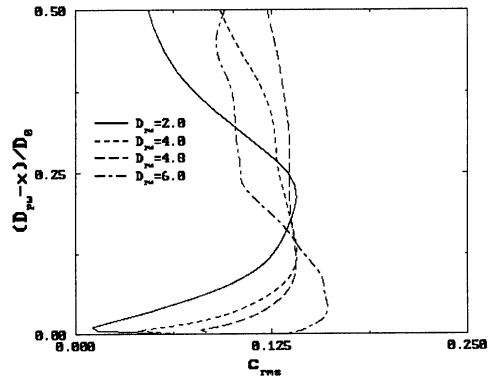

Figure 4. Rms of concentration fluctuations at 1.0 D_0 from the jet centreline

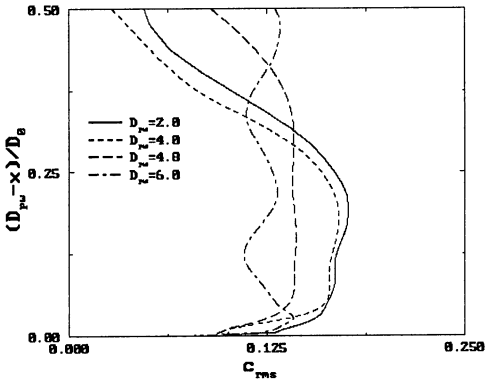

Figure 5 Rms of concentration fluctuations at 2.0 D_0 from the jet centreline

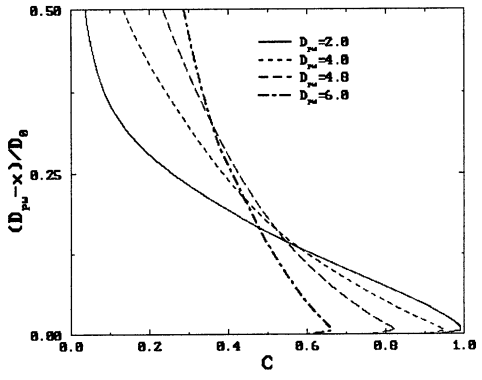

Figure 6. Average concentration at 1.0 D_0 from the jet centreline

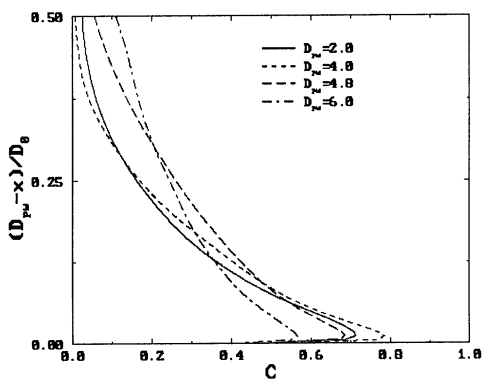

Figure 7. Average concentration at 2.0 D_0 from the jet centreline

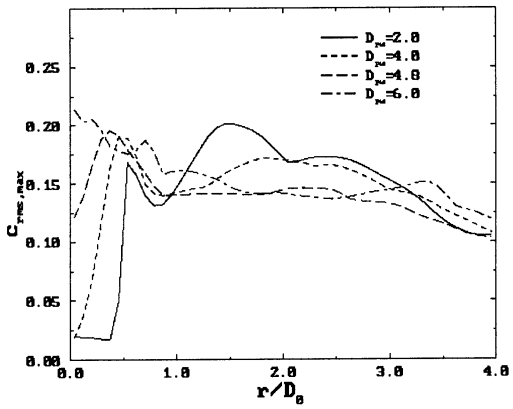

Figure 8. Maximun rms. of concentration fluctuations along the radial wall jet

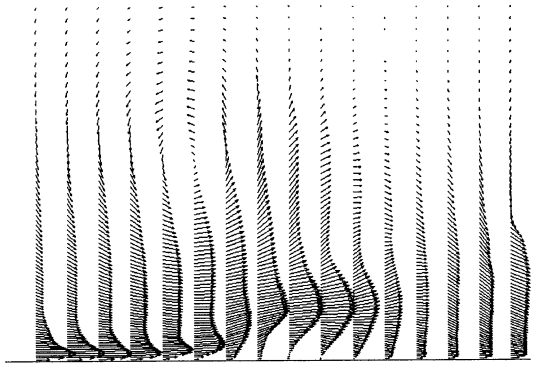

Figure 9. Instantaneous velocity field in the wall jet.

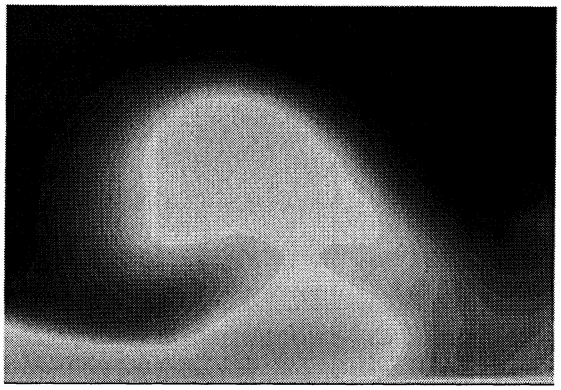

Figur3 10. Instantaneous concentration field. Lighter areas denote higher concentration

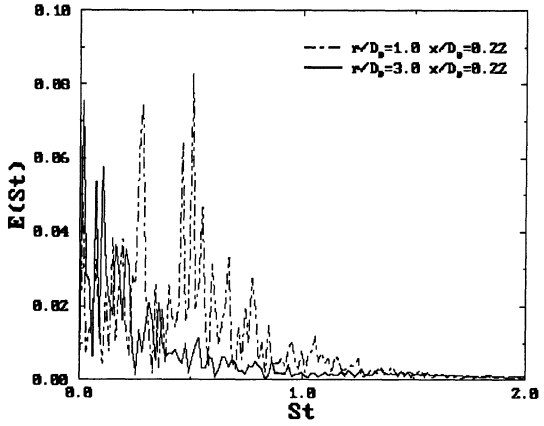

Figure 11. Spectral density of concentration fluctuations at two locations in the wall jet for D_{pw}=2.0

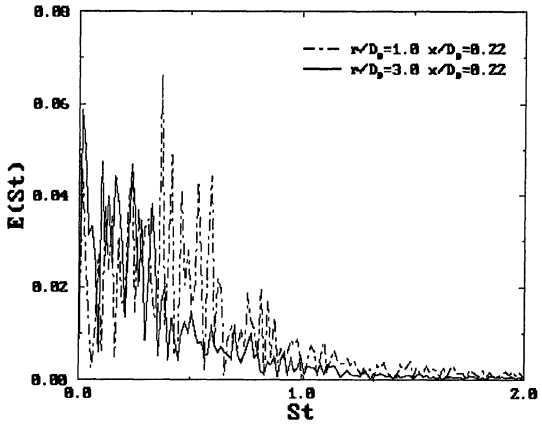

Figure 12. Spectral density of concentration fluctuations at two locations in the wall jet for D_{pw}=4.0